THEORETICAL AND EXPERIMENTAL STUDY OF THE ELASTOPLASTIC BEHAVIOR OF THE CASTOR OIL POLYURETHANE (RICINUS COMMUNIS).

Amauri Bravo Ferneda, amauri@utfpr.edu.br
Romeu Rony Cavalcante da Costa, romeu@utfpr.edu.br
Federal University of Technology - Parana – Department of Mechanical Engineering

Abstract. *Biopolymers have been widely used as alternative materials to attend the performance requirements that the medical area has demanded for bone implants. In this way, the Castor Oil Polyurethane (Ricinus communis) has taken a distinct place. Nevertheless, this material, considered bone constructive, still needs a consistant mechanical investigation for a reliable application, despite the great difficulty to predict the mechanical behavior of biopolymer structures. Face this fact, this work intends through experiments in normalized specimens for tensile and compressive tests, as well as normalized tests for hip implants, to obtain material properties and mechanical behavior data required to implement computational models of the hip prosthesis. Using the finite element method, computational simulations are carried out to verify the capability of Drucker-Prager material model to represent the biopolymer mechanical behavior. This model was first applied in tensile and compressive tests simulations, and further in prosthesis biopolymer simulations, where more complex loadings are present. The results of these simulations are analyzed and discussed in order to validate the use of this material model in biopolymers structures.*

Keywords*: biopolymer; material model; experimental tests; finite element analysis, hip prosthesis.*

1. INTRODUCTION

During the last century, humanity has improved the quality of living conditions, so, the life expectancy has increased. This situation has occurred, mainly, due to technological advances in different research areas (Etchebehere, 1998). For example, surgeries for bone reconstitution are more common, because the population is getting older (Wregge, 2000), and the bone implants must attend satisfactorily the functions executed by the part removed. Therefore, the structure implanted needs to support the requirements of service and to minimize the problems of rejection. An alternative way to solve these requirements consists of the use of biopolymers to manufacture the prosthesis like that shown in the work developed by Katti (2004). According to Ereno (2003), a biopolymer obtained from the castor oil polyurethane (*Ricinus communis*), developed by Chemistry Institute of São Carlos, is biocompatible and the possibility of rejection is very low. However, it is important to mention that this work does not discuss the aspects related to biological studies. In fact, the focus is on the application of material models in order to simulate the mechanical behavior of the biopolymer obtained from the castor oil polyurethane (*Ricinus communis*).

 The castor oil polyurethane (PU) has been used in many applications, such as in dental implants (Vianna, 1997), wood adhesives (Jesus *et al.* 1998), concrete agglomerates (Silva, 1998), bone defect filling (Ignácio, 1999), bone cement (Pascon, 1999), hip prostheses (Silvestre Filho, 2001), electrical insulators (Murakami, 2002); vegetal fiber composite matrixes (Silva, 2003), and intrapatellar socket gloves (Bonini, 2004). In Ferneda *et al.* (2006), the authors presented the mechanical behavior of Castor Oil Polyurethane *(Ricinus communis)* under high strain rate, uniaxial compression conditions. Costa *et al.* (2009) has carried out a study under monotonic tests in order to make a preliminary investigation of the creep phenomenon; cyclic tests. At present, experimental tests for hip prosthesis are performed under monotonic tests to evaluate elastoplastic behavior of this biopolymer.

Thus, for the application of models, it was necessary to determine the material properties, as well as to understand the behavior of the biopolymer. In this sense, specimens were manufactured following the standards published by American Society for Testing and Materials. After, tensile experimental tests were carried out for monotonic tests in order to make a preliminary investigation of the creep phenomenon; cyclic tests were also performed. Therefore, in this work, the parameters of material models obtained from the experimental results and from monotonic tests for hip prosthesis were included at the program Abaqus™ and finite element analyses were performed and computational results were compared to the experimental results.

2. MATERIALS AND METHODS

The biopolymer is synthetic polyurethane from a castor oil of *Ricinus communis*. The polyurethane is constituted by two components called pre-polymer 329L and poliol 471. In order to obtain the biopolymer, it is necessary to mix one portion of pre-polymer 329L to 0.7 portion of poliol 471 in mass. Using this mixture, fill the cavities of the flexible molds to produce the specimens used in the tensile test (ASTM D638-96 Type I), compression (ASTM D695-96) and stem hip (ISO 7206-3 and ISO 7206 - 4).

2.1. Experimental part

The experimental tensile test is outlined in Costa et al. (2009) and Figure 1 (a) is shown as the body-of-evidence test under monotonic tensile displacement of 0.8 mm / min and measurements were made with the aid of strain gages. In Figure 1 (b) is shown one of the curves of stress-true strain obtained from these tests.
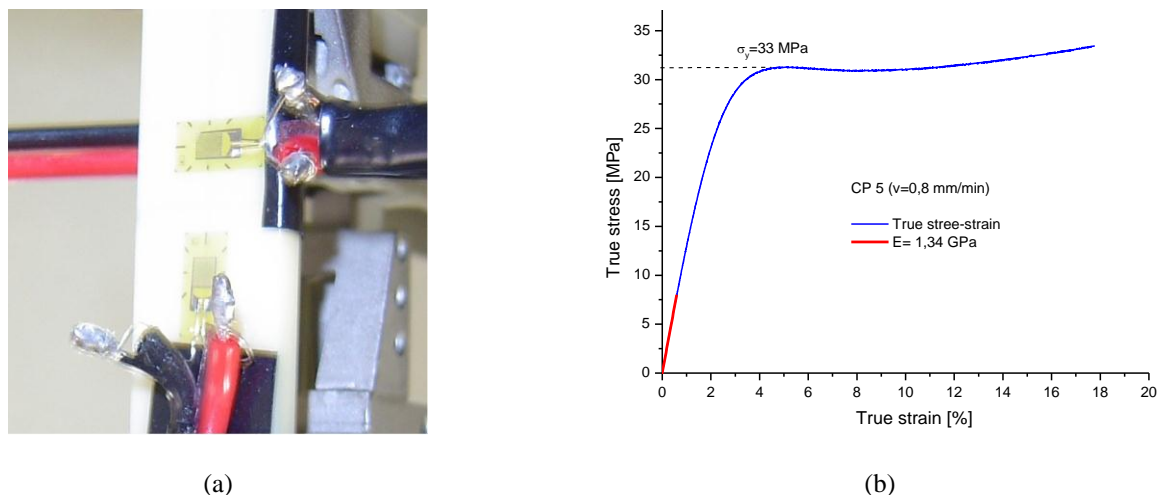

| (a) | (b) |

Figure 1. (a) monotonic tensile test under 0.8 mm / min, (b) Results: Young´s modulus and yield stress in this test.

The experimental test compression is detailed in Ferneda et al. (2006) and Figure 2 (a) is shown in test under monotonic compressive displacement of 0.8 mm / min, where one can notice that the specimen undergoes a minimum barrel, portraying the physical behavior expected for this type of material and testing and in Figure 2 (b) is one of the resulting curves displayed in this test. In this test, the stress is obtained with the aid of the strain-gage bonded to the transverse direction that is able to measure the circumferential strain. Therefore, one can calculate the variation of cross-sectional area of the CP (specimen) and get instant active tension, which is the ratio between the applied force and the instantaneous cross-sectional area. It appears initially that the curve is free of non-linearity between 0% and 0.5% true strain, because it was directly measured in the CP. Moreover, the value of the modulus of elasticity is higher, reaching 1.56 GPa, which shows the influence of machine stiffness in previous trials. Finally, it should be noted that the value of yield stress was reduced due to the calculation of the instantaneous stress acting.
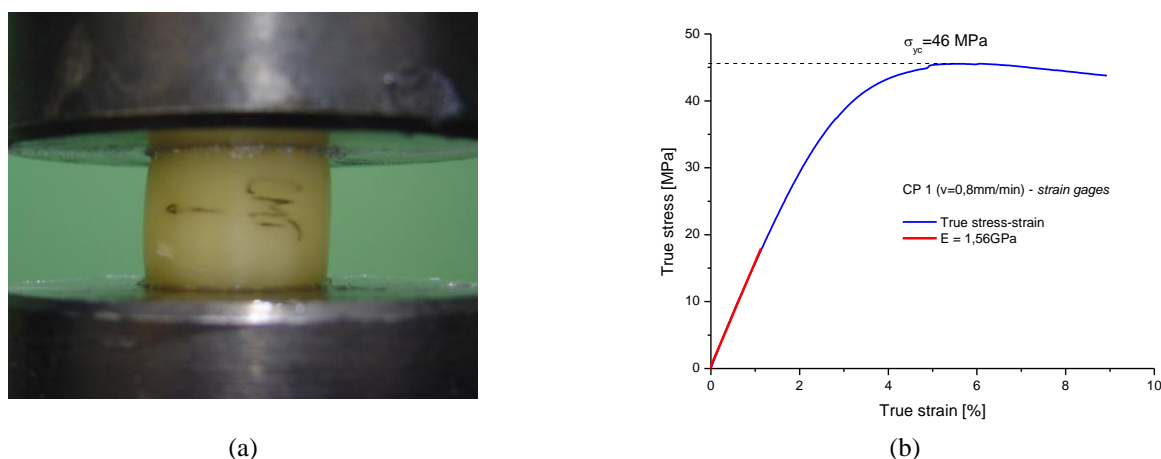

| (a) | (b) |

Figure 2. (a) monotonic compressive test under displacement of 0,8 mm/min; (b) Results: Young´s modulus and yield stress in this test.

Tests were carried out to evaluate of hip implant joint behavior. Figure 3 (a) shows the beginning of the test of hip prosthesis according to ISO 7206-3, which requires the application of a force always normal in relation to the alumina ball attached to the tip of the prosthesis and a force´s line always passing the center of the ball. The bearing slides on the track, keeping the vertical direction of the force, aligned with the center of the ball to the end of the test (Figure 3 (b)).

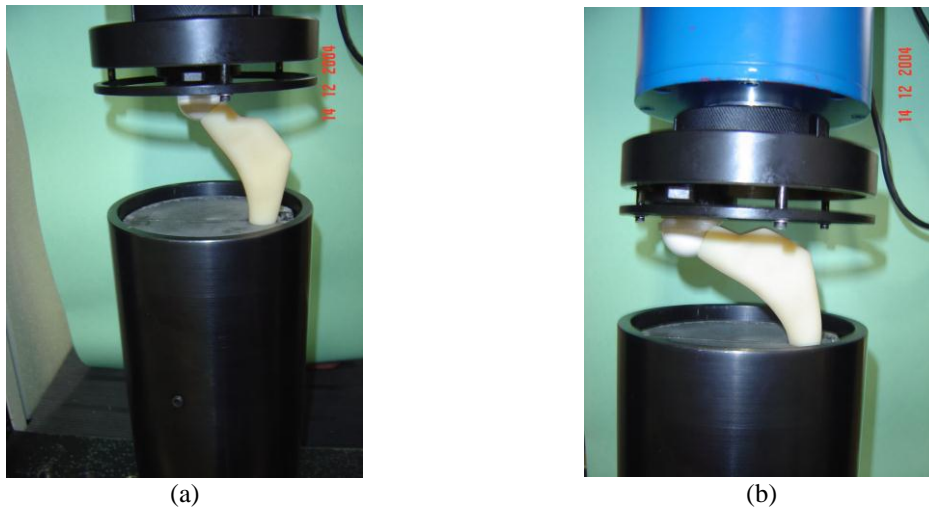<div align="center">(a)   (b)</div>

Figure 3. Test according to ISO 7206-3: (a) beginning, (b) final.

Figure 4 shows the load-displacement curves obtained from tests with the test device, shown in Figure 3. As noted earlier, there is also a little linear behavior displayed by the prosthesis at the beginning of the trial, approximately 400 to 500N, as theoretically expected and as a result of the earlier experiments. Above that, there is a nonlinear behavior. There is an increase of loading up to about 700 N, and after this value there is a considerable loss of stiffness.
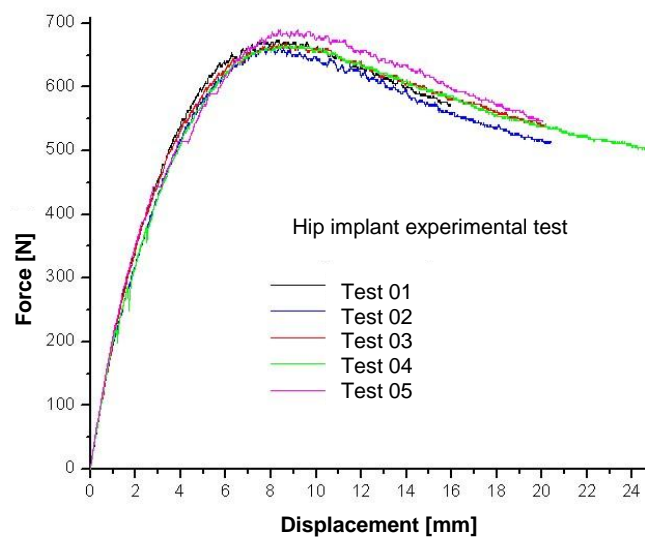

Figure 4. Load-displacement curve: velocity 0,8 mm/min (ISO 7206-3)

2.2. Computational part

Material Model

All computer models made for this study were developed in ABAQUS® program, specifically the version 6.3.1, using the finite element method. The selection of this application was made thanks to the formulation of the model have all the Drucker-Prager implemented (Hibbit et al. 2000). Therefore, based on results of laboratory tests in speed of 0.8 mm/min, we determined the parameters associated with the Drucker-Prager model.

An alternative to obtain the parameters associated with the Drucker-Prager model is by determining the parameters of the Mohr-Coulomb failure usually used to analyze brittle materials. The Mohr-Coulomb model is based on the Mohr circles defined by maximum and minimum principal stresses. Thus, the fault line model is the best straight line that touches these circles, defining the parameters c (cohesion) and ϕ (internal friction angle) (Figure 5).
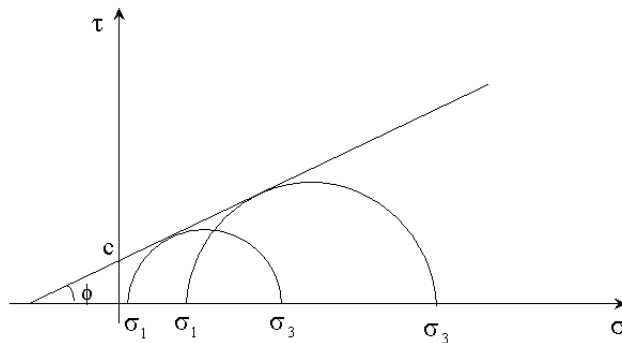
Figure 5 - Model of Mohr-Coulomb failure (Hibbit et al., 2000).

The parameters c and φ can be determined by the values of tensile and compressive material, provided it is used with some geometrical relationships. Thus, we have:

$$\sin \phi = \frac{|\sigma_c| - \sigma_T}{|\sigma_c| + \sigma_T} \qquad (1)$$

$$c = \frac{1 + \sin \phi}{2 \cos \phi} \qquad (2)$$

Where:

σ_c = stress of compressive strength

σ_T = stress of tensile strength

However, the Mohr-Coulomb model assumes that the failure independent of the intermediate values of the principal stress and the same is not true with the Drucker-Prager model. Therefore, it is possible to verify the difference that exists between the two models by Figure 6, since the Mohr-Coulomb model presents vertices when projected in the Plane-π. This implies that small changes in stress can cause significant changes in the direction of plastic flow.

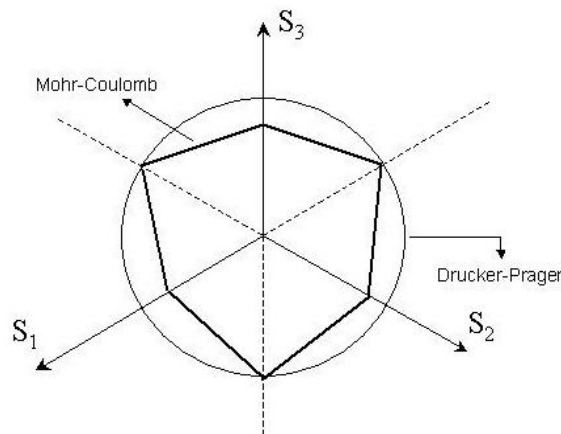Figure 6 - Mohr-Coulomb criterion and Drucker-Prager-designed Plan π (Hibbit et al. 2000).

According to Hibbit et al. (2000), if used as an analysis under plane strain condition, it follows that the parameters of Drucker-Prager parameters are related to the Mohr-Coulomb by the following equations:

If $\quad \psi = \beta \quad$ then $\quad \tan \beta = \dfrac{\sqrt{3} \sin \phi}{\sqrt{1 + \dfrac{1}{3} \sin^2 \phi}} \quad , \quad \dfrac{d}{c} = \dfrac{\sqrt{3} \cos \phi}{\sqrt{1 + \dfrac{1}{3} \sin^2 \phi}} \qquad (3)$

If $\quad \psi = 0 \quad$ (incompressible) then $\quad \tan \beta = \sqrt{3} \, \text{sen} \, \phi \quad , \quad \dfrac{d}{c} = \sqrt{3} \cos \phi \qquad (4)$

The above expressions show that for values ϕ above 50°, we see that the parameters of Drucker-Prager parameters are very close to the Mohr-Coulomb.

Typically, one has σ_C correspond to the resistance under compression and σ_T is the tensile strength. But for the present work σ_C corresponds to the yield stress under compression and σ_T corresponds to the yield stress in tension because the biopolymer showed a ductile behavior in both the tensile and compression tests. Whereas the biopolymer will respect the rule of associativity shown in Table 1, it has equal values for angle of dilation (ψ) and friction angle (β) (associativity: $= \psi \ \beta$) for the parameters of Drucker-Prager . The calculation was done by taking the average value of tensile stress and compressive tests recorded. The average values of tension were obtained $\sigma_T = 31.422$ MPa for tension and $\sigma_c = 42.54$ MPa for compression, and the strain averages were 10.47% and 14.18% for tension and compression, respectively. By using these values in the calculation of coefficients the values of 36.14 and for cohesion 24.28° friction angle were obtained (shown in Table 1).

Table 1. Values of Parameters of Drucker-Prager.

Parameters	Value
Angle of friction (β)	24,28°
Cohesion (d)	36,14 MPa
Dilation angle (ψ) (Assossiativity: $\psi = \beta$)	24,28°

For the linear model of Drucker-Prager, used in the analysis, while it inserts the values of β and ψ, it is necessary to put another parameter (K) called the rate of flow stress (flow stress ratio) . According to Hibbit et al. (2000), this parameter should be between $0.778 \leq K \leq 1.0$ to ensure the convexity of the surface of lamination. By the establishment of $\psi = \beta$ as well as K = 1, the original model of Drucker –Prager (Hibbit et al. 2000) returns.

Apart from determining the parameters of Drucker-Prager, it is necessary to obtain the plastic stress-strain curve (true) to express the evolution of work hardening, which is inserted in the "Drucker Prager Hardening". However, determining the stress-strain curve after the "necking" is not a simple task because it involves a triaxial stress field, so the tension in the direction of loading needs to be corrected. If the CP is cylindrical traction, you can use the method of correction procedure proposed by Bridgman (1952), where tension is adjusted according to the radius of curvature of necking and the radius of the current cross-section of CP. However, the CP has tested prismatic shape and the assumptions used by Bridgman (1952) are not valid in this case (Ling, 1996).

Then, in order to determine a more realistic strain hardening curve, we sought out literature methods for obtaining the same. It should be noted that most of these methodologies are the type numerical-experimental, or involve testing and computational modeling. Among the papers, there are the methods proposed by: Ling (1996), Zhang et al. (1999), Zhang et al. (2001); Cabezas and Celentano (2004). However, all these methods were employed for metallic materials, using well Model Mises. In this study, we adopted the methodology proposed by Ling (1996), but the material model used was the Drucker-Prager.

The methodology proposed by Ling (1996) consists of finding a curve by considering isotropic hardening of two constitutive laws: the Law of Power and a Linear Law, given by:

$$\text{Power law: } \sigma_v = \left(\frac{\sigma_{vu}}{\varepsilon_{vu}^{\varepsilon_{vu}}} \right) \varepsilon_v^{\varepsilon_{vu}} \tag{5}$$

$$\text{Linear law: } \sigma_v = \sigma_{vu} \left(1 + \varepsilon_v - \varepsilon_{vu} \right) \tag{6}$$

Where:

ε_{vu} = true strain at the beginning of "necking"

σ_{vu} = true stress at the beginning of "necking"

According to Ling (1996), the Power Law underestimates the real hardening law while the Linear Law overestimates. Consequently, the Power Law can be considered a Lower Boundery curve, and the Linear Law can be considered an Upper Boundery curve, so that the hardening law, "almost real", would be between these boundery curves (Figure 7).
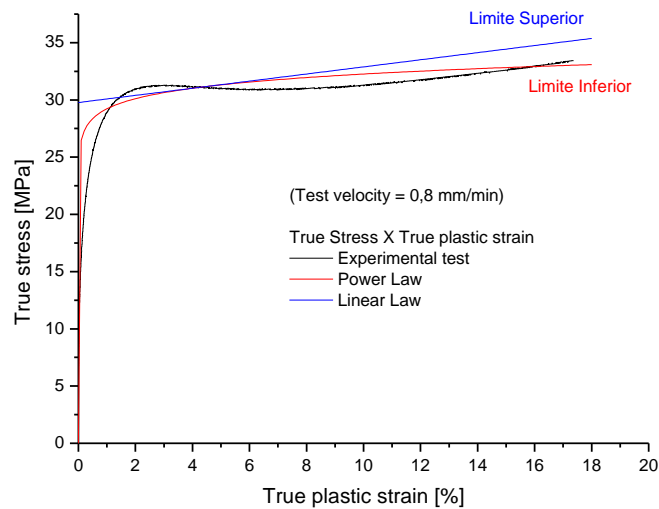
Figure 7 - Curves Upper Limit and Lower Limit biopolymer.

Therefore, a hardening law "almost real" can be estimated by weighting these two constitutive laws:

$$\sigma_v = \sigma_{vu}\left[w\left(1 + \varepsilon_v - \varepsilon_{vu}\right) + \left(1 - w\right)\left(\frac{\varepsilon_v^{\varepsilon_{vu}}}{\varepsilon_{vu}^{\varepsilon_{vu}}}\right)\right] \qquad (7)$$

Where w is the weighting factor, given the limits between zero and one, and if w is zero, the curve of strain hardening is given by a Power Law. If w equals 1, the hardening curve is given by a linear law. Finally, if w lies between 0 and 1, the hardening curve is given by examining the two laws. Thus, the most important aspect of the methodology is the determination of w. To this end, we use the model in Figure 4, the criterion of Drucker-Prager laminating, and apply it as the initial estimate, the hardening law given by equation (7), considering w equal to 0.5 (Figure 8) .
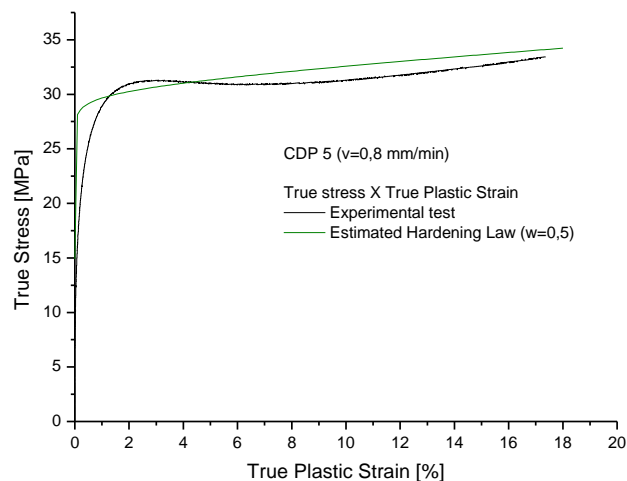

Figure 8 - Tensile strain hardening curve estimated for the biopolymer (w = 0.5).

This compares well to load-deflection curve of engineering numerically with the experimental curve in order to check if the parameter w needs to be adjusted. If this is necessary, you should change the law hardening and simulate again. This interactive procedure occurs until the force is calculated computationally closer to the measured force. In short, the load-deformation curve of engineering is used to calibrate the weighting factor w.

Computational analysis of the hip stem implant

Initially, in order to verify the capabilities and constraints of the Drucker-Prager model in representing the mechanical behavior of biopolymer under this type of loading, computational analysis were performed simulating the tensile test (Costa et al. 2009) and compression (Ferneda et al.2006).

It was observed that the same treatment given during the test was imposed on the model, i.e., the resultant force applied on the rod should go through the center of the sphere. With considerations implemented in the model of this work, such requirements have been met as can be seen from Figure 9 that shows the set in position undisturbed (Figure 9 (a)) and the deformed position (Figure 9 (b)), where the acetabulum always remains in its normal position in relation to the ball. In the modeling of hip joint implants, acetabular-rod-sphere, it follows that the sphere of alumina was attributed to the linear-elastic properties: tensile modulus equal to 366 GPa and Poisson's ratio equal to 0.22 (WREGGE, 2000).
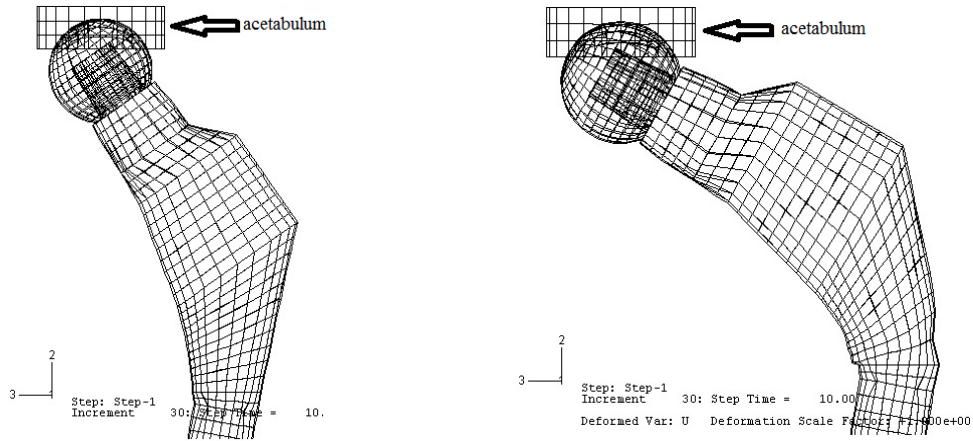
(a) beginning of the analysis, undeformed;   (b) in the final analysis, deformed
Figure 9 – Position of hip prosthesis.

The hip prosthesis and the acetabulum, both made from the biopolymer, were modeled based on the results of laboratory tests in a speed of 0.8 mm / min for tension and compression. Since the test of the rod implant that is used is guided by the flexion, the flexural module was used as information of elastic property (E_1^f) in supplying the CAE program, based on the values already mentioned.

According to Carlsson & Pipes (1987) for this type of case, we use the apparent flexural modulus. From equation 8, it is possible to calculate the apparent flexural modulus as a function of the properties of pure tension and compression:

$$E_1^f = \frac{2E_t}{1 + \sqrt{E_t / E_c}} \qquad (8)$$

Thus, as we have values of E_t and E_c for the modules of tension and compression, respectively, using equation 8, we obtain a value of $E_1^f = 1.375$ GPa. Therefore, the calculated value recommended is intermediate to those obtained for tensile and compression. This value was used for the computational analysis of the test rod.

The curve of evolution is introduced in the characteristic "Drucker-Prager Hardening" in Drucker-Prager model in the form of pairs as shown in Table 2.

Table 2 – Values of true stress-strain plastic:

True Stress (MPa)	Plastic true strain
28.94437	0.00
29.37160	0.002
29.82726	0.004
30.11299	0.006
30.32771	0.008
30.50300	0.01
31.11696	0.02
31.90464	0.04
33.02644	0.08
34.80279	0.16
35.60575	0.2
49.62848	1.00

3. RESULTS AND DISCUSSIONS

In the modeling of contact on the ball-joint acetabulum two conditions were tested: finite sliding and sliding small (Hibbit et al. 2000). The finite sliding option was one that achieved a better representation of the conditions observed in experimental testing. It may be noted that the displacement of the acetabulum in the vertical direction proceeded with the proper positioning of both elements from the beginning to the end of the analysis. As to the burden due to displacement of the parts, the direction of its resultant passes through the center of the ball throughout the test. With considerations implemented in the model of this work, such requirements have been met as can be seen from Figure 9 that shows the set in position undisturbed (Figure 9 (a)) and the deformed position (Figure 9 (b)), where the acetabulum always remains in its normal position in relation to the ball.

For the analysis of hip implants three types of conditions of contact to the whole acetabulum-sphere were tested. In one of them, called "Frictionless", the presence of friction between these two elements is disregarded. As a second option, called "Penalty", the existence of friction between the two parts was admitted, in which it was assumed a coefficient of 0.3, which can be considered high. In the third case-study, called "Static-Kinematic Exponential Decay" estimated values of 0.1 for the static friction, of 0.015 for a cinematic and a reduction rate of 0.001 between them are used. In Figure 10 are presented the analysis of situations with variations of friction, and in them all the contact surfaces between the ball and acetabulum was assumed to be finite sliding. Thus, in Figure 10 it is noticed that the options mentioned are somewhat similar in behavior.
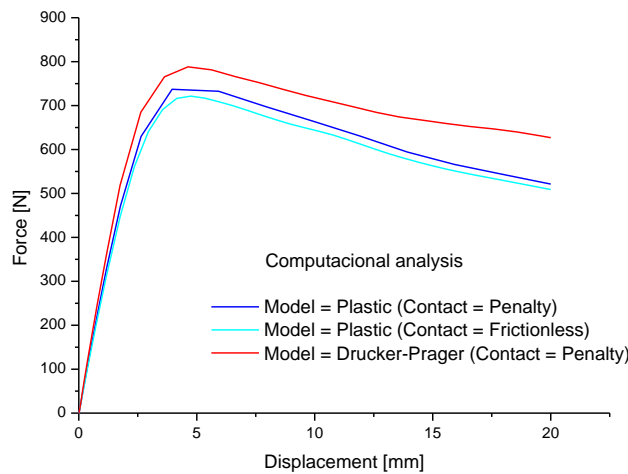

Figure 10 - Load-displacement curve comparison: Plastic Model X Drucker-Prager Model.

Under the qualitative aspect, the numerical results show that the model of prosthetic-device set and the boundary conditions imposed at the same, are reasonable to simulate the tests specified by ISO 7206-3 (Figure 11).

(a)   (b)
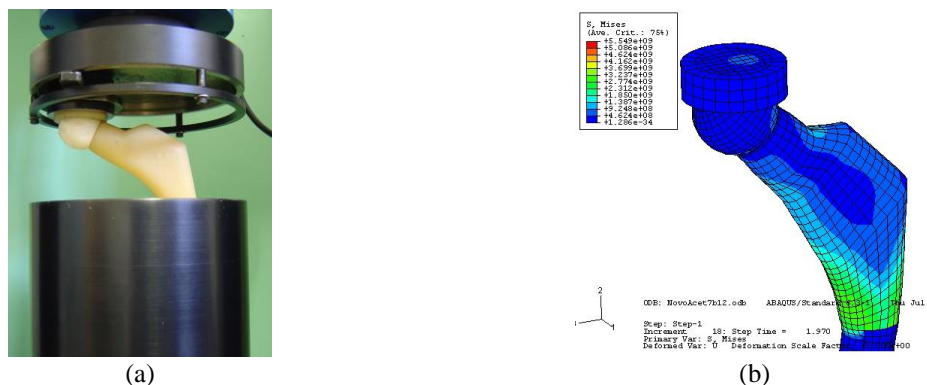Figure 11 - Test according to ISO 7206-3: (a) Experimental test; (b) Computational analysis.

However, by Figure 12 one can see that the results of simulations using the Drucker-Prager model does not explicitly express those obtained with the experimental. It may be noted that the curves obtained from the computational data are representative of the phenomenon of softening of the biopolymer.
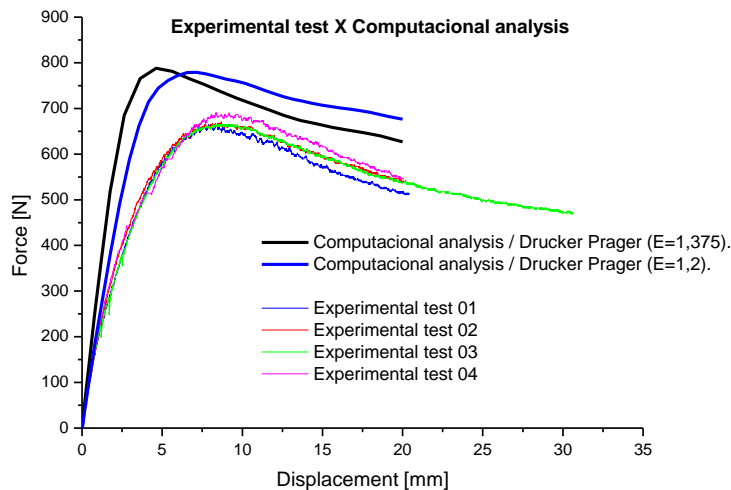
Figure 12 - Load-displacement curve comparison: experimental result Drucker-Prager x result.

We conducted a test to reduce the value of modulus of elasticity of 1.375 to 1.2 in order to analyze the model sensitivity to this parameter. It was noted that the numerical curve tended towards the experimental.

Thus, in addition to the model of Drucker-Prager material, we tested the "Plastic" for insertion of material models which uses the von Mises criterion (Hill). Data input consists of the elastic properties of the material modulus and coefficient of Poison, added to the stress-strain curve for expressing the true plastic strain hardening in the evolution of the biopolymer, shown in Table 2. Figure 13 shows a comparison between the force versus displacement curve for Drucker-Prager, Von Mises (with different contact cases) and experimental tests.
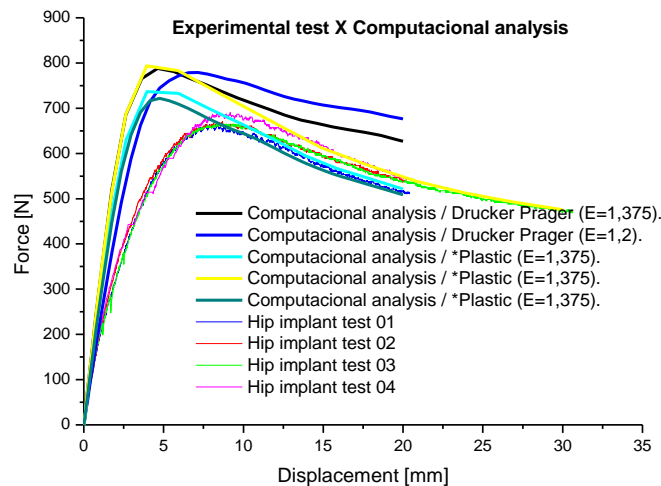

Figure 13 - Load-displacement curve comparison: experimental result x numeric result.

4. CONCLUSIONS

Under the qualitative aspect, the numerical results show that the model of prosthetic-device set and the boundary conditions imposed at the same are reasonable to simulate the tests specified by ISO 7206-3.

The finite sliding option was one that achieved a better representation of the conditions observed in experimental testing.

In the simplification adopted by the computational analysis in the region of attachment between the rod and the device, there is the imposition of nodal restrictions on the type "ENCASTRE", which doesn't allow any kind of strain on that region. Thus, when comparing both of the curves, experimental testing versus computational analysis, it's possible to note the existence of certain distance between them. The computational results of tension show that the Druker – Prager Model with the perfect plasticity curve was able to represent reasonably the behavior of the polymer up to 11% of strain. Above this value, the polymer had a certain degree of hardening with the presence of the "necking" phenomenon and therefore, an estimated hardening curve was adopted by a numerical-experimental methodology. The obtained results showed that the methodology is valid, however, it can be improved with the inclusion of equations that may contemplate the "softening" phenomenon as well as visco-elastic effects.

5. REFERENCES

Astm D 638 – 96, 1996. Standard Test Method For Tensile Properties Of Plastics. West Conshohocken.

Astm D 695 – 96, 1996. Standard test method for compressive properties of rigid plastics. West Conshohocken.

Bonini S., 2004. Estudo comparativo da resistência transversal, resistência à compressão, dureza superficial e comportamento visco-elástico da resina poliuretana em relação à resina acrílica usada para prótese dental. [Doctorate Thesis]. Ribeirão Preto: University of São Paulo.

Bridgman, P. W. , 1952. Studies in large plastic flow and fracture. Harvard University Press, Cambridge-Massachusetts.

Carlsson, L. A.; Pipes, R. B., 1987. *Experimental characterization of advanced composite materials.* PRENTICE-HALL, INC. Englewood Cliffs, New Jersey, USA.

Costa, R. R. C., 2007. "Aplicabilidade de modelos constitutivos para analisar o comportamento mecânico de um biopolímero". 171p. Tese (Doutorado) - Escola de Engenharia de São Carlos, Universidade de São Paulo, São Carlos, Brazil.

Costa, R. R. C.; Ferneda, A. B.; Tita, V., 2009. "Study of mechanical behavior for a biopolymer: experimental tests and numerical simulations". Proceedings of the 20th International Congress of Mechanical Engineering. Gramado, Brazil.

Ereno, D., 2003. Polímero derivado de óleo vegetal, sintetizado por químico de São Carlos, ganha mercado internacional. Pesquisa Fapesp. Edição 91. Setembro.

Etchebehere, E. C. S. C., 1998. Recentes Avanços em Densitometria Óssea. Jornal do Médico. Pp. 7.

Ferneda, A. B., 2006. "Estudo Teórico-experimental do Comportamento Elastoplástico do Poliuretano Derivado do Óleo de Mamona (Ricinus Communis)". 135p. Tese (Doutorado) - Escola de Engenharia de São Carlos, Universidade de São Paulo, São Carlos, Brazil.

Ferneda, A. B.; Costa, R. R. C.; Tita, V.; Proença, S. P. B.; Carvalho, J.; Purquerio, B. M., 2006. "Compression tests of castor oil biopolymer". Mat. Res. [online]. vol.9, n.3, pp. 327-334. ISSN 1516-1439.

Hibbit, Karlsson & Sorensen. 2000. *ABAQUS Theory Manual.* v2. Version 6.1.

Ignácio, H., 1999. *Avaliação da poliuretana da mamona nas formas compacta e porosa no preenchimento de falha óssea: Estudo experimental em cães*. [Doctorate Thesis]. Ribeirão Preto: University of São Paulo.

ISO 7206-3, 1988. Implants for surgery - Partial and total hipjoint prostheses - Part 3: Determination of endurance properties of stemmed femoral components without application of torsion.

ISO 7206-4, 1989. Implants for surgery - Partial and total hip joint prostheses - Part 4: Determination of endurance properties of stemmed femoral components without application of torsion.

Jesus, J. M. H, Calil Júnior, C.; Chierice G. O., 1998. Adesivo a base de óleo de mamona para madeiras. *Proceedings of the XIII Congresso Brasileiro de Engenharia e Ciência dos Materiais; Curitiba, Brazil*; Curitiba; pp. 2063-2971.

Katti, K. S., 2004. Biomaterials in total joint replacement. Colloids and Surfaces B: Biointerfaces. n39. p 133–142.

Ling, Y., 1996. Uniaxial true stress-strain after necking. AMP Journal of Technology, v.5, p.37-48.

Murakami, C. R., 2002. *Aplicações das resinas poliuretanas derivadas do óleo de mamona, como materiais isolantes elétricos*. [Doctorate Thesis]. São Carlos: University of São Paulo.

Pascon, E. A., 1999. *Projeto biocompatibilidade dos materiais endodônticos: Biocompatibilidade da resina poliuretana derivada da mamona*. [Doctorate Thesis]. Ribeirão Preto: University of São Paulo.

Silva, I. J., 1998. *Contribuição ao estudo da utilização da resina poliuretana a base de óleo de mamona na construção civil*. [MSc Dissertation]. São Carlos: University of São Paulo.

Silva, R. V., 2003. *Compósito de resina poliuretano derivado de óleo de mamona e fibras vegetais*. [Doctorate Thesis]. São Carlos: University of São Paulo.

Silvestre Filho, G. D., 2001. *Comportamento mecânico do poliuretano derivado de óleo de mamona reforçado por fibra de carbono: contribuição para o projeto de hastes de implante de quadril*. [MSc Dissertation]. São Carlos: University of São Paulo.

Vianna, D. L., 1997. *Estudo comparativo da resistência mecânica da poliuretana derivada de óleo vegetal submetida à ensaios de tração*. [MSc Dissertation]. Ribeirão Preto: University of São Paulo.

Wregge, P. A. S., 2000. Metodologia para obtenção de esferas de cerâmica para próteses de quadril. São Carlos, 186p. Tese (Doutorado). Escola de Engenharia de São Carlos – Universidade de São Paulo.

Zhang, Z.L.; Hauge, M.; Odegard, J.; Thaulow, C., 1999. Determining material true stress-strain curve from tensile specimens with rectangular cross-section. International Journal of Solids and Structures, v.36, p.3497-3516.

Zhang, Z.L.; Odergard, J.; Sovik, O.P., 2001. Determining true stress-strain curve for isotropic and anisotropic materials with rectangular tensile bars: method and verifications. Computational Materials Science, v.20, p.77-85.

6. RESPONSIBILITY NOTICE